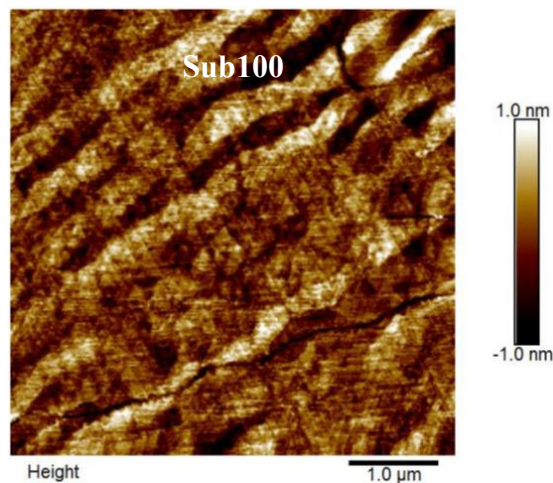
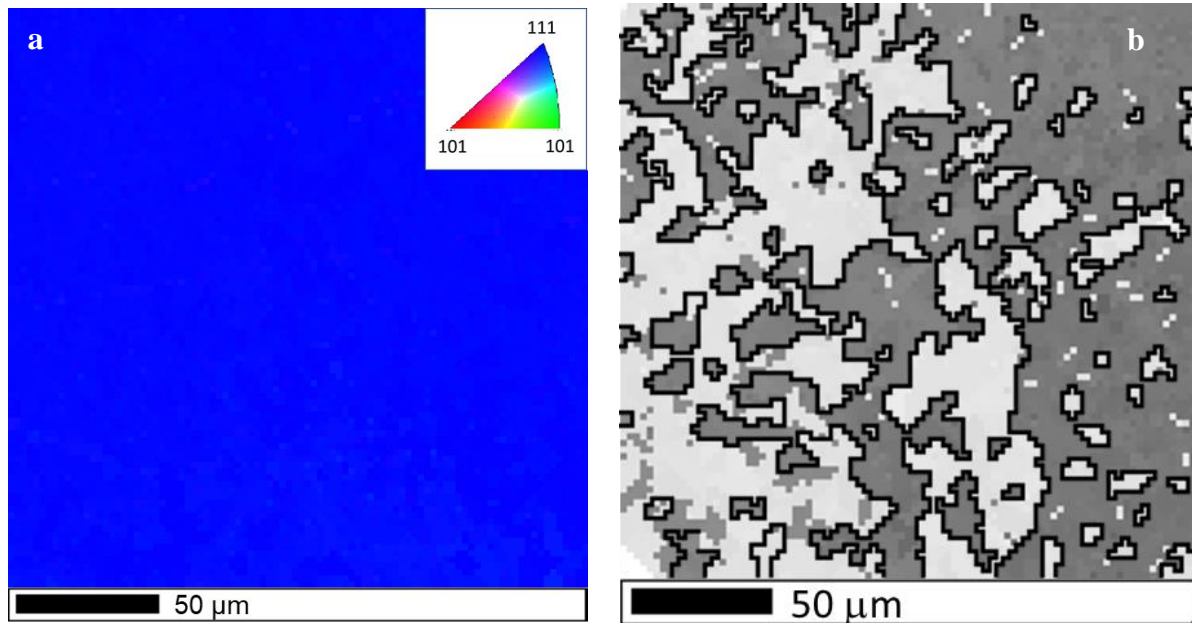


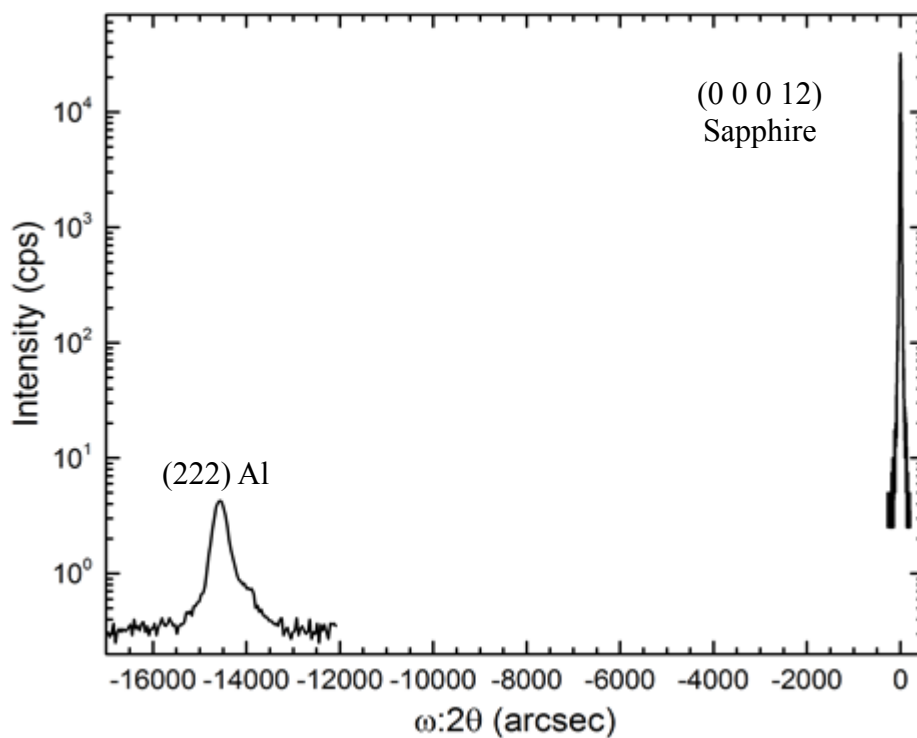
Supplementary Figure 1. Schematic diagram of crystal structure of Al and sapphire. For (111) Al, distance between adjacent Al atoms = $d_{[110]} = 2.863583 \text{ \AA}$. Distance between adjacent O atoms = $(2/3)d_{[10\bar{1}0]} = 2.747733 \text{ \AA}$. The mismatch is $\sim 4\%$ if the Al metal aligns with the O from sapphire.¹ Note that images are to scale and color difference is to show clarity between Al from metal and sapphire.



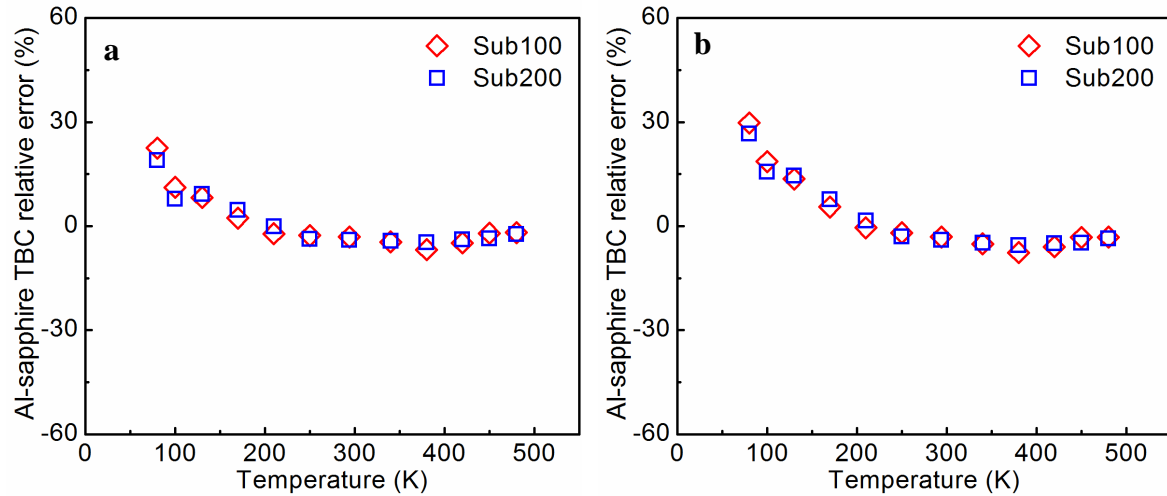
Supplementary Figure 2. Atomic Force Microscopy (AFM) images of Al surface. Root-mean-square (RMS) roughness for a $5 \mu\text{m} \times 5 \mu\text{m}$ area is 0.288 nm for Sub100. The scale bar is $1 \mu\text{m}$.



Supplementary Figure 3. **a** Electron back-scattered diffraction (EBSD) image of Sub200 showing only (111) oriented Al. The inset shows the legend for the stereographic projection. The EBSD was measured in an FEI Quanta 3D FEG Dual Beam (SEM/FIB) system with an HKL EBSD attachment. The data was obtained with HKL fast acquisition software. The scale bar is 50 μm . **b** The in-plane orientation shows the presence of twinning. Higher angle grain boundaries are not observed, confirming that both Sub200 and Sub100 are (111) with the average un-twinned $> 20 \times 20 \mu\text{m}^2$. The scale bar is 50 μm .



Supplementary Figure 4. Triple-axis diffraction results of Sub100. The experimental conditions of triple-axis diffraction on Sub100 are, detector slits: 1375" divergence, Al FWHM: 251", Step: 30", Count: 360 sec. The (222) Al is -14565" away from the (00012) Al_2O_3 peak so the experimental $a(\text{Al}) = 4.0422 \pm 0.0007 \text{ \AA}$ while an Al powder measurement using the same equipment is $4.04236 \pm 0.00009 \text{ \AA}$. Therefore, Al film in Sub 100 (and Sub 200) is strain-free.



Supplementary Figure 5. **a** the relative errors of the measured TBC comparing with the Landauer TBC. **b** the relative errors of the measured TBC comparing with the AGF TBC.

Supplementary Notes

The supporting information includes the schematic diagram of the crystal structure of Al and sapphire (Supplementary Figure 1), the AFM scanning image of the surface of Sub100 (Supplementary Figure 2), EBSD image of Sub200 showing only (111) oriented Al (Supplementary Figure 3), the in-plane orientations of the Al films showing the presence of twinning, triple-axis diffraction results of Sub100 (Supplementary Figure 4) showing that Al film in Sub 100 (and Sub 200) is strain-free, the relative errors of the measured TBC comparing with the Landauer TBC and AGF TBC (Supplementary Figure 5), and calculation details of the AGF and Landauer modelling.

Supplementary Methods

AGF. Briefly, the system (Supplementary Fig. 6) could be separated into three parts: two semi-infinite leads (L & R) and a finite size central region(C). In this case, L is bulk Al, R is bulk

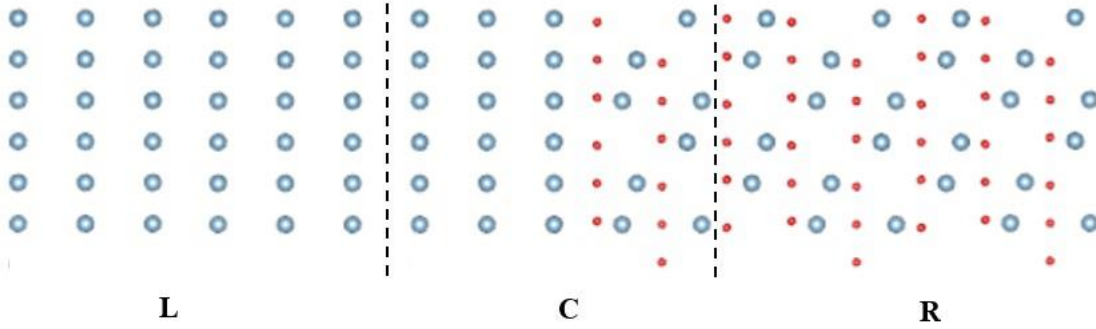
sapphire. Supplementary Fig. 6 is plotted via VESTA.² Under harmonic assumption, the transmission function of the system is

$$\Xi(\omega) = \mathbf{Tr}(\Gamma_L(\omega)G_C(\omega)\Gamma_R(\omega)G^\dagger(\omega))$$

where $\Gamma_{\alpha=L,R}$ is the level-width function of the leads and G_C is the Green's function of the central region. Subsequently, the thermal conductance could be obtained from

$$\sigma(T) = \int_0^\infty \hbar\omega \frac{\partial f(\omega, T)}{\partial T} \Xi(\omega) \frac{d\omega}{2\pi}$$

where $f(\omega, T)$ is the Bose-Einstein distribution.



Supplementary Figure 6. Schematic of the Al-sapphire system. L, C and R mean left lead, central region and right lead, respectively.

As for thermal conductance, we used a modified thermal conductance expression to reflect the temperature drop right across the interface rather than between two heat reservoirs.³

$$\sigma'(T) = \sigma(T) \times \frac{1}{1 - 0.5 \times \left[\frac{\sigma(T)}{\sigma_1(T)} + \frac{\sigma(T)}{\sigma_2(T)} \right]}$$

where σ_1 and σ_2 are the thermal conductance of pure material of both leads, and σ is the thermal conductance of the interface.

Calculation details about non-equilibrium Landauer approach. For the modeling of the non-equilibrium Landauer approach, the second order force constants of both Al and sapphire are obtained from first-principle calculations within the framework of density functional theory (DFT), as implemented in the Vienna Ab initio Simulation Package (VASP). The phonon dispersion curves of Al [111] and sapphire [0001] orientations are calculated with Phonopy from force constant files from VASP. Other phonon properties (like phonon modal group velocity, phonon density of states) of Al and sapphire are achieved from phonon dispersion curves with MATLAB. For the DFT calculation of Al, the supercell is $4 \times 4 \times 4$ Al primitive cell and the k-mesh is $3 \times 3 \times 3$. For the DFT calculation of sapphire, the supercell is $2 \times 2 \times 2$ sapphire primitive cell and the k-mesh is $4 \times 4 \times 4$. The exchange–correlation energy functional for our DFT calculation is with the generalized gradient approximation (GGA) of Perdew, Burke, and Ernzerhof (PBE). The transmission coefficients are obtained from the diffuse mismatch model (DMM) with only phonon properties of Al and sapphire from DFT.

Supplementary References

- 1 Medlin, D., McCarty, K., Hwang, R., Guthrie, S. & Baskes, M. Orientation relationships in heteroepitaxial aluminum films on sapphire. *Thin Solid Films* **299**, 110-114 (1997).
- 2 Momma, K. & Izumi, F. VESTA 3 for three-dimensional visualization of crystal, volumetric and morphology data. *J. of Appl. Crystallograph.* **44**, 1272-1276 (2011).
- 3 Tian, Z., Esfarjani, K. & Chen, G. Enhancing phonon transmission across a Si/Ge interface by atomic roughness: First-principles study with the Green's function method. *Phys. Rev. B* **86**, 235304 (2012).